Crosstalk-free all-optical switching enabled by Fano resonance in a multi-mode photonic crystal nanocavity

Saudan, Quentin; Bekele, Dagmawi A.; Dong, Gaoneng; Yu, Yi; Yvind, Kresten; Mørk, Jesper; Galili, Michael

Published in:
Optics Express

Link to article, DOI:
10.1364/OE.449588

Publication date:
2022

Document Version
Publisher's PDF, also known as Version of record

Research Article Vol. 30, No. 5 / 28 Feb 2022 / Optics Express 7457
Optics EXPRESS

Crosstalk-free all-optical switching enabled by Fano resonance in a multi-mode photonic crystal nanocavity

QUENTIN SAUDAN,[1,*] DAGMAWI A. BEKELE,[1] GAONENG DONG,[1] YI YU,[1] KRESTEN YVIND,[1,2] JESPER MØRK,[1,2] AND MICHAEL GALILI[1]

[1]DTU Fotonik, Technical University of Denmark, DK-2800 Kongens Lyngby, Denmark
[2]NanoPhoton - Center for Nanophotonics, Technical University of Denmark, Denmark
[*]ques@fotonik.dtu.dk

Abstract: We demonstrate all-optical switching using a multi-mode membranized photonic crystal nanocavity exploiting the free-carrier induced dispersion in InP and the sharp asymmetric lineshape of Fano resonances. A multi-mode cavity is designed to sustain two spatially overlapping modes with a spectral spacing of 18 nm. The measured transmission spectrum of the fabricated device shows multiple asymmetric Fano resonances as predicted by optical simulations. The capabilities of the device are benchmarked by comparing a wavelength conversion from 1538.2 nm to 1565.2 nm with a single-mode wavelength conversion at 1566.2 nm on the same device. The results show an improvement in signal quality with a 5.6 dB power penalty reduction at the receiver as well as in energy efficiency with a reduction of the pump power from 534 fJ/bit to 445 fJ/bit.

1. Introduction

Photonic crystal nanocavities(PhCN) have shown to greatly enhance the optical electromagnetic field confinement and the light-matter interaction, giving rise to strong optical nonlinearities [1]. Combined with the low linear loss of waveguides achievable in semiconductors like indium phosphide(InP) or silicon(Si), nanocavities can be used for energy efficient signal processing on optoelectronic chips. Indeed, all-optical switching with nanocavities offers improved performance due to a faster processing speed along with reported record low energy consumption of less than a femtojoule of switching energy [2], while reducing the number of optical-electrical-optical domain conversions. In addition, the data can be transferred in optical waveguides on longer distances, which removes the need for long energy-hungry electrical interconnects [3]. Various optical operations such as all-optical switches [4], all-optical memories [5], pulse carving [6] and demultiplexer [7,8] have been demonstrated at high-speed and low energy in similar photonic structures.

It has been shown that all-optical switching can be enhanced by modifying the lineshape of the resonance using a Fano resonator [9,10]. As observed and discussed in many different topics of physics [11,12], the Fano resonance arises from the interference of a continuum of states with a discrete one, e.g. a continuum of waveguide modes with a discrete nanocavity mode in the case of photonic crystals(PhC) [13]. So far, such a scheme has been used in the case of a single-mode lattice-shifted cavity, also known as H0 cavity, showing promising high-speed and low energy all-optical switching in InP [14]. But it still suffers from the inherent proximity between the pump and probe optical frequencies, and therefore from a strong in-band crosstalk. This is inadequate for a practical on-chip integration as it will involve very accurate filtering of the pump and potentially require an error correction step to compensate for the added crosstalk.

#449588 https://doi.org/10.1364/OE.449588
Journal © 2022 Received 16 Dec 2021; revised 2 Feb 2022; accepted 13 Feb 2022; published 18 Feb 2022

Optics EXPRESS

Two-mode or cross-mode all-optical switching solves the proximity issue by having the pump and signal aligned to two different modes with engineerable spectral separation. Such a configuration has already been demonstrated in an L4 multi-mode cavity [15] or a photonic molecule with two coupled H0 single-mode cavities [16]. Here, we demonstrate a device which combines the sharp asymmetric lineshape of the Fano resonance with a multi-mode H1 cavity and achieve crosstalk-free all-optical switching between the L- and C-band at 2.5 Gbps.

2. All-optical switching

As shown in the Fig. 1(a), the interference between the waveguide and the cavity paths, with the addition of a partially transmitted element, generates the sharp asymmetric transmission Fano lineshape seen in Fig. 1(b). By pumping the nanocavity with a pulsed signal, the resonance can be shifted due to non-linearities such as optical Kerr effect and free-carrier induced dispersion, which is composed of both band-filling effects and plasma dispersion [17]. The resonance shift is affecting the probe by changing its transmission through the device from an OFF(low probe transmission in solid black) to an ON(high probe transmission in dashed grey) state as shown in Fig. 1(b). This scheme has been successfully used for the on-chip optical processing of on-off keying(OOK) signals in operations such as wavelength conversion [18], optical time domain demultiplexing [8] or optical sampling [19].

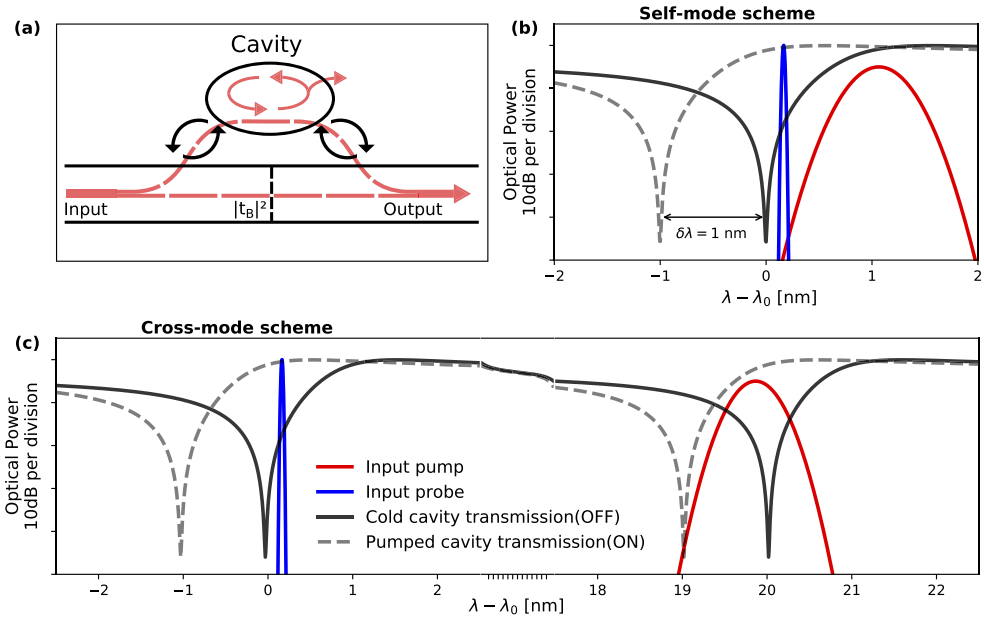

Fig. 1. **(a)** Schematic illustration of the theoretical configuration used to generate Fano resonance lineshapes with a cavity side-coupled to a waveguide. The red arrows depict the path of the light through the device. **(b)** Schematic illustration of self-mode all-optical switching with a single-mode cavity in the spectral domain. The solid black and dashed grey lines depict the transmission of an asymmetric Fano resonance device in the OFF and ON states respectively. The blue curve corresponds to the input CW probe and the red one is the broad input pulsed pump. **(c)** Schematic illustrations of a cross-mode configuration with the pump and probe separated by 20 nm and interacting through a dual-mode cavity. The transmission spectra are calculated using standard temporal couple mode theory(TCMT) for a single-mode and dual-mode cavity. The lower axis is aligned to the wavelength of minimum transmission of the cold probe cavity mode and has a different scaling between 3 nm and 17 nm for a continuous view. .

Optics EXPRESS

Here, we introduce a different method for all-optical switching by making use of a multi-mode cavity instead of a single-mode cavity. In Fig. 1(b), a single resonance is both pumped and used to modify the continuous-wave(CW) probe transmission in a configuration we refer to as self-mode. It shows a tight spectral proximity between the probe and pump. The latter needs to be filtered out and therefore introduces inherent limits to the self-mode scheme : the pump cannot be positioned to the wavelength of maximal cavity coupling, increasing the energy consumption and limiting the spectral bandwidth(hence modulation speed) of the pump. In addition, the filtering of the pump will be difficult after the device, leading to considerable in-band crosstalk. These limits can be overcome by using a cross-mode scheme where pumping and probing happen at two different resonances of a multi-mode cavity. In Fig. 1(c), the pump is placed at a second cavity resonance engineered to be 20 nm apart from the probe cavity resonance. In this configuration, the pump does not leak into the probe bandwidth and can be filtered out completely by, for example, a distributed Bragg reflector, avoiding the need for narrowband sharp tunable filters, which would increase the complexity and power consumption of the device. Additionally, the pump can be placed at the wavelength of maximum cavity coupling, holding promise for decreasing the pumping energy. The coupling between the two modes arises from the common change of refractive index of the material in the cavity. In the case of InP nanocavities, the fast local diffusion of free-carriers generated by two-photon absorption(TPA) in the pump mode leads to a refractive index change of the probe mode due to the plasma dispersion induced by these free-carriers. It is expected that the intensity profile of the modes should overlap maximally to give an efficient switching mechanism.

3. Device

The optical switch is realized in-house as a 2D photonic crystal membrane on an InP-on-insulator platform. The details of the fabrication are thoroughly discussed in [20]. The InP provides a good combination of low loss and strong free-carrier effects at 1550nm. Light is coupled in and out of the chip through uniform photonic crystal grating couplers with 6.5 dB loss each and guided to the photonic crystal, where the switching occurs, using wire waveguides. The light is then guided by a line-defect waveguide and coupled to a multi-mode H1 cavity as shown in the SEM image of Fig. 2(a). The waveguide-cavity coupling is modified by a partially transmitting element(PTE) as an additional hole in the waveguide, giving rise to the particular asymmetric Fano resonance lineshapes [21] that can be observed on the measured transmission spectrum in Fig. 2(d).

The different airhole shifting parameters, the hole radius and the lattice parameter of the PhC are adjusted using three dimensional finite difference time domain(3D FDTD) simulations to obtain a combination of good cavity Q factors, good mode overlap and suitable resonance frequencies to be compatible with C-band to L-band wavelength conversion. The chosen values are $C1 = 0.222$, $L1 = 0.129$, $a = 495$ nm, $r = 138$ nm and the PTE is shifted by $a/2$ to the left from the vertical axis of symmetry. The electric intensity profile $|\boldsymbol{E}|^2$ of the final intrinsic modes are shown in Fig. 2(b-c) and their respective origin is deduced from [22] to be quadrupole and hexapole. By fitting the experimental data to the standard temporal coupled mode theory for 3 modes and 3 ports [23], as shown by the dashed red line in Fig. 2(d), we can extract the total quality factor Q_{tot} of each of the modes and their exact resonance wavelength. The fitting accuracy is limited by the wavelength dependent scattering matrix of the PTE, which is unknown for this specific device and is extracted from 3D-FDTD simulations. The relevant properties for the modes used for all-optical switching are listed in Table 1. Notice that the center quadrupole mode is not characterized in depth as it was not considered for all-optical switching due to its low total Q factor and extinction ratio. The mode volume is calculated with the standard expression

$$V = \frac{\iiint \epsilon(\boldsymbol{r})|\boldsymbol{E}(\boldsymbol{r})|^2 d^3\boldsymbol{r}}{max(\epsilon(\boldsymbol{r})|\boldsymbol{E}(\boldsymbol{r})|^2)} \tag{1}$$

Optics EXPRESS

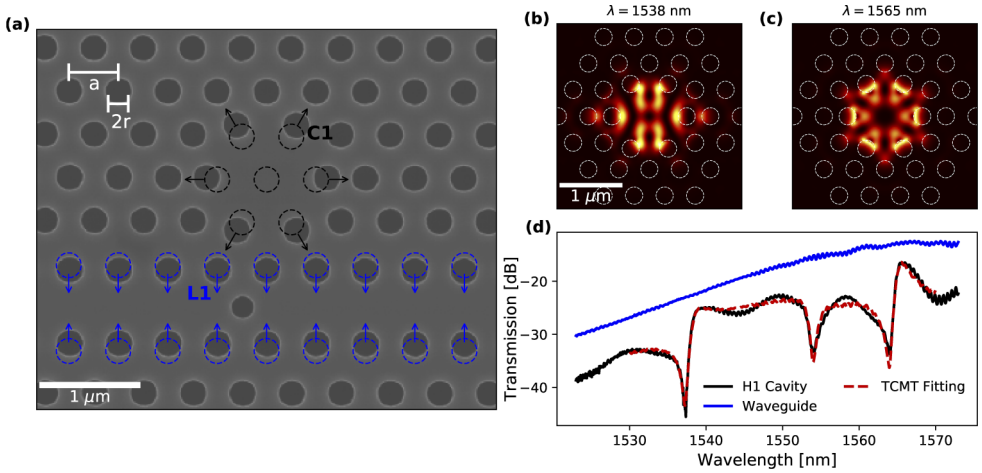

Fig. 2. **(a)** SEM image of the Fano resonance structure with a multi-mode H1 cavity. The hole shifting parameters C1 and L1 are shown with arrows. **(b-c)** Electric field intensity profiles $|\boldsymbol{E}|^2$ of the two main cavity modes with overlayed photonic crystal structure in the intrinsic case. Calculated with 3D FDTD simulations. **(d)** Transmission spectrum of the fabricated device with three noticeable cavity resonances in black. An analytical model is fitted to it using temporal coupled mode theory(TCMT) and shown in dashed red. The blue line is the grating coupler transmission optimized for a maximum transmission for the L-band resonance around 1566 nm.

where $\epsilon(\boldsymbol{r})$ is the dielectric constant of the structure and $E(\boldsymbol{r})$ is the field profile of the investigated mode.

Table 1. Characteristics of the two main modes in the designed H1 cavity. The total Q factors are extracted by fitting TCMT spectra to the transmission of an experimental H1 cavity transmission, whereas the mode volumes and intrinsic Q factors are calculated based on 3D-FDTD simulations of the intrinsic cavity.

	λ_0 [Fit]	Q_{tot} [Fit]	Q_{in} [3D-FDTD]	Mode Volume [3D-FDTD]
Mode 1	1538.2 nm	900	5′270	0.698 $(\lambda/n)^3$
Mode 2	1565.2 nm	1250	54′000	0.76 $(\lambda/n)^3$

The mode volumes shown in the Table 1 are larger than the standard single-mode lattice-shifted H0 cavity [24], which might affect the relaxation of the cavity. Indeed, the main speed limitation of a switch based on carrier-induced dispersion is the decay of the carriers due to the diffusion and the surface recombination. The diffusion is directly influenced by the mode profile and mode volume, which modifies the short time scale relaxation of the carriers [25]. In order to characterize the speed potential of the device, we perform a pump-probe measurement of the cavity relaxation on the 1538 nm resonance and compare it to a single-mode H0 cavity. The experimental setup used is explained in [26]. The relaxation of both cavity types is shown in Fig. 3 where the transmission of the probing laser is plotted for each pump-probe delay and normalized to the maximum of transmission. As the measured time trace depends on both the asymmetric lineshape of the resonance and the free-carrier relaxation, it is not straightforward to extract carrier relaxation time constants. However, we can readily conclude using the raw or the filtered data that the H1 cavity has a longer relaxation time than the H0 in the self-mode configuration. Therefore, we expect the switching mechanism to be slower than 10 GHz. Note that this limitation is due to the intrinsic properties of the cavity and not to the type of scheme,

Optics EXPRESS

i.e. self- or cross-mode, used for the wavelength conversion. Because of the slower relaxation of the H1 cavity, we performed the wavelength conversion experiment at a rate of 2.5 GHz.

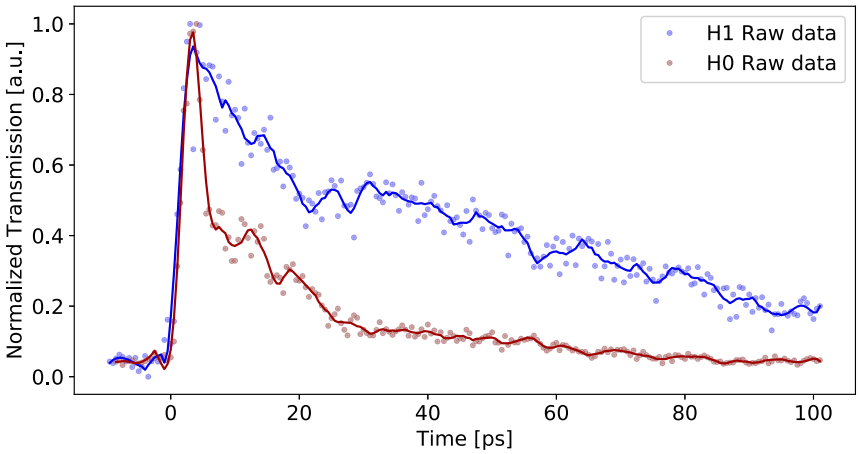

Fig. 3. Relaxation of the resonance shift for the H0 and H1 cavity in a self-mode configuration. The dots correspond to the raw data and the lines are smoothed versions of the data using a Savitzky-Golay filter. The lines are to be used as a guide for the eye.

As previously mentioned, the overlap between the pump and probe mode is a determining factor for the cross-mode modulation. Indeed, since the two modes will have different mode profiles, the TPA-generated carriers might not overlap well with the probe mode and give a negligible refractive change to the probe mode, hence a negligible modulation of the probe. The amount of free-carrier leading to the refractive index change of a specific mode is defined as the weighted average of the local free-carrier density $N(\boldsymbol{r}, t)$ by the probing mode profile $\boldsymbol{E}(\boldsymbol{r})$

$$N_{eff} = \frac{\iiint N(\boldsymbol{r}, t)\epsilon(\boldsymbol{r})|\boldsymbol{E}(\boldsymbol{r})|^2 d^3\boldsymbol{r}}{\iiint \epsilon(\boldsymbol{r})|\boldsymbol{E}(\boldsymbol{r})|^2 d^3\boldsymbol{r}} \tag{2}$$

By comparison, the profile of the generation rate of free-carriers due to TPA is proportional to $|E|^4$ [25]. Therefore, we define the following overlap integral to estimate the efficiency of the cross-mode modulation process :

$$OI(U_1, U_2) = \frac{\left(\iiint U_1(\boldsymbol{r})U_2(\boldsymbol{r})d^3\boldsymbol{r}\right)^2}{\iiint U_1(\boldsymbol{r})^2 d^3\boldsymbol{r} \iiint U_2(\boldsymbol{r})^2 d^3\boldsymbol{r}} \tag{3}$$

with $U_1(\boldsymbol{r})$ and $U_2(\boldsymbol{r})$ two arbitrary real scalar fields and apply it to $|\boldsymbol{E}|^4$ and $|\boldsymbol{E}|^2$. The overlap integral is 1 if $U_1(\boldsymbol{r}) = U_2(\boldsymbol{r})$ for the integrated volume. We apply this integral in the self-mode and cross-mode case with the pumping(λ = 1538 nm) and probing(λ = 1565 nm) modes shown in Fig. 2(b-c) and find that $OI(|\boldsymbol{E}_{pump}|^4, |\boldsymbol{E}_{pump}|^2)$ = 84% in the self-mode case and $OI(|\boldsymbol{E}_{pump}|^4, |\boldsymbol{E}_{probe}|^2)$ = 46% in the cross-mode case. We therefore expect the switching process to be less energy efficient in the cross-mode case for an equivalent cavity power, which can be compensated by having a much better coupling of the pump to the cavity mode as the pump can be placed at the resonance wavelength in the cross-mode configuration.

Optics EXPRESS

4. Experiment

4.1. Experimental setup

As a benchmark for all-optical switching, the wavelength conversion of an OOK signal from C-band to L-band is demonstrated using the experimental setup depicted in Fig. 4. The pump is generated by a mode locked laser(MLL) at a 10 GHz pulse rate. The spectrum is broadened in a highly nonlinear fiber(HNLF) and subsequently filtered by a waveshaper(WSS) to match with the frequency of the cavity resonance. The 10 GHz pulses are modulated by a lithium niobate Mach-Zehnder modulator with a 2.5 Gbps 2^{15} pseudo-random bit sequence generated from an Anritsu bit pattern generator(BPG). The rate reduction from 10 GHz to 2.5 GHz is performed by setting a specific pattern on the BPG with words of 4 bits, each containing 1 PRBS bit and 3 zero bits. The resulting signal is a 2.5 Gbps return-to-zero on-off keying(RZ-OOK) signal with a 5% duty-cycle and 20 ps long pulses that can be accommodated by the device under test.

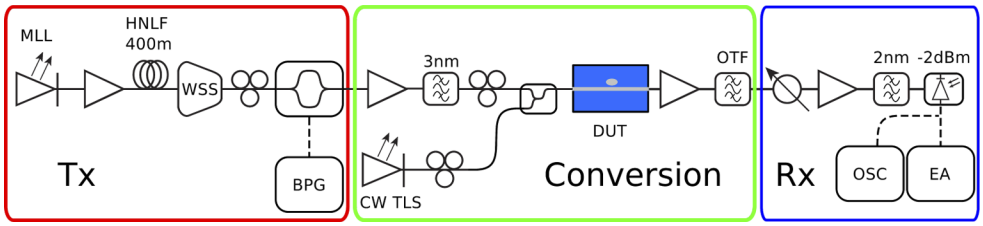

Fig. 4. Scheme of the experimental setup used for the wavelength conversion of a RZ OOK signal. The red box is the transmitter generating the pumped signal, the green box corresponds to the wavelength conversion stage and the blue box is the receiver. MLL is mode-locked laser. WSS is waveshaper. BPG is bit pattern generator. EA is error analyser. OTF is optical tunable filter. CW TLS is a continuous-wave tunable laser source. Solid and dashed lines correspond to optical and electrical signals respectively.

The pump signal is reamplified by a high power C- or L-band erbium-doped fiber amplifier(EDFA), combined with the CW probe and coupled to the chip via cleaved fibers and grating couplers. After wavelength conversion with all-optical switching, the output is preamplified by an L-band EDFA to compensate for the grating coupler losses and the pump is filtered out by an optical tunable filter(OTF). The final signal is sent to a 10 GHz photodiode and analysed by an error analyser(EA) for bit-error rate(BER) measurement. A 50 GHz photodiode is also used to detect the fast cavity response with an Agilent 13GHz 40 GS/s digital storage oscilloscope(DSO). The clock used by both the BPG and EA is recovered before the waveshaper and sent to a second 10 GHz photodiode.

4.2. All-optical switching with H1 cavity

In order to show the improvement in signal quality and energy efficiency of the proposed all-optical scheme, we perform a wavelength conversion through the all-optical switching of the 2.5 Gbps signal in both a self-mode and cross-mode configuration using the same H1 cavity. As the two resonances are in different optical band, different optical amplifiers with similar noise figures are used. We chose to keep the probe fixed in the L-band resonance around 1565 nm and have a fixed setup after the DUT with an L-band EDFA for amplification and a similar detection wavelength. By filtering the broadened MLL pulses either at 1566 nm or 1539 nm, we can select the pumped cavity mode and use respectively a self-mode or cross-mode configuration for the wavelength conversion. The respective input spectra to the device are shown in Fig. 5(a) and (b).

In both cases, the probe is not set at the minimum of transmission, which would be the optimal point for a maximum contrast between the ON and OFF states. This is due to the thermal

Optics EXPRESS

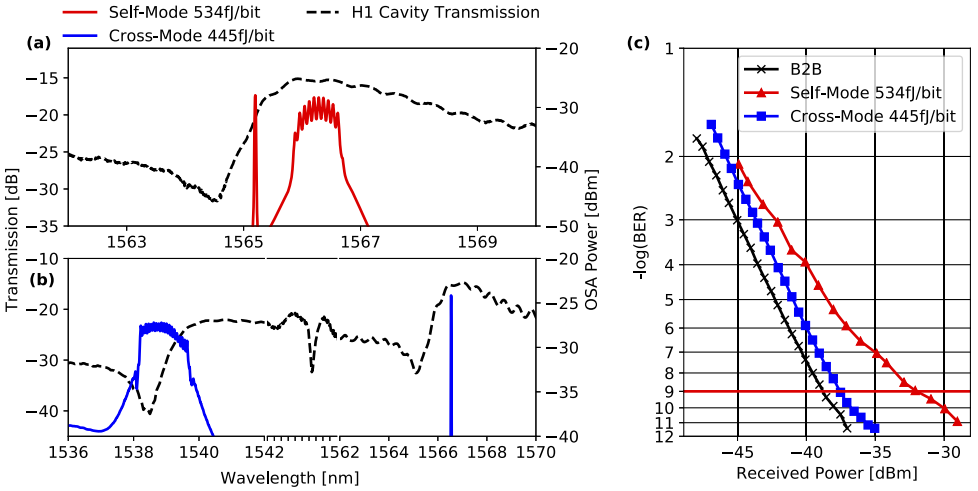

Fig. 5. **(a-b)** Spectra taken at the input of the device for self-mode and cross-mode configuration are shown with the transmission of the device with H1 cavity in dashed black line. The broad signal corresponds to the modulated pump and the narrow one to the CW probe. **(c)** BER versus the received power for the self-mode and cross-mode configuration compared to the back-to-back.

red-shifting of the cavity. Indeed, during all-optical switching operation, heat is generated by the free-carrier and two-photon absorption in the cavity and red shifts the relaxed state of the cavity. This effect is shown in the Supplement 1. Since the heating process speed is of the $1-10\ \mu$s [27] order and the plasma dispersion of the 100 ps order in such photonic crystal cavities, we assume the dynamic modulation is not affected by these thermal effects.

We report a consistent improvement of the signal quality in the cross-mode configuration with a 5.6 dB power improvement with respect to the self-mode at the receiver for a BER of 10^{-9} and a minor power penalty of 0.9 dB with respect to the back-to-back(Fig. 5(c)). We attribute this improvement to the suppression of the pump intraband crosstalk. In addition, the pump pulse energy requirement is reduced as a result of three competing effects. On one side, a lower Q/V ratio(Table 1) for the pump mode at 1538 nm in the cross-mode case decreases the confinement of the light and therefore the TPA generation, which should result in an increase in energy consumption. In addition, the overlap between the pumping and probing mode is smaller in the cross-mode configuration as shown with Eq. (3), again increasing the required pulse energy. These effects are counterbalanced by a much better coupling of the pump to the cavity in the cross-mode case since the pump can be placed at the resonance wavelength of the pump mode. In overall, a slight reduction of the pump pulse energy from 534 fJ/bit to 445 fJ/bit is observed. At equivalent Q/V ratio of the pump mode or mode overlap, this improvement is expected to be more significant.

The output signals for both self- and cross-mode modulations are shown in Fig. 6(a) and we can observe a clear 2.5 GHz spacing between the modulation side-bands. In the case of self-mode(blue spectrum), we also observe additional side-bands with a similar spacing. This interfering signal corresponds to the pump, broadened by the cavity switching, which leaks in the filtering band of the probe and cannot be removed. A zoomed-out version of the unfiltered spectra in Fig. 6(b) shows the proximity of the broadened pump and the probe in the self-mode case. The wavelength shift of the probe between the experiments is due to the known oxidization of the cavity during operation leading to a blue shift of the cold cavity resonance and has been shown to be eliminated with atomic layer deposition [28].

Optics EXPRESS

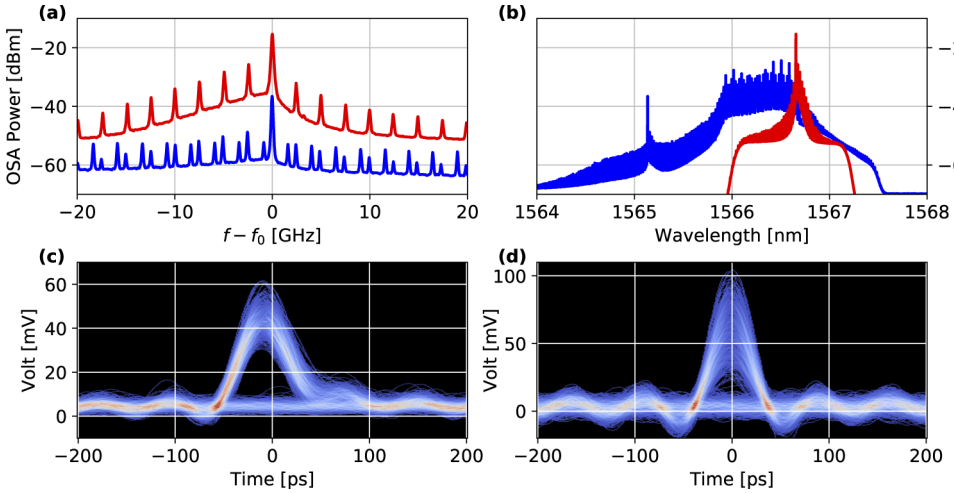

Fig. 6. **a)** High-resolution spectra of the output modulated signal centered at the probe wavelength for the self-mode(blue) and cross-mode(red) experiment. **b)** Full unfiltered spectrum showing the pump and probe in blue and the probe in red for their respective cases. **b)** and **c)** Eye diagrams respectively for cross-mode and self-mode experiments at −37.9 dBm received power.

The interference seen in the spectral domain is also observed in the time domain. The eye diagrams shown in 6(c) and (d) are acquired at a received power of −37 dBm and confirm the BER measurement : in the cross-mode case(c), we observe a clear eye-opening corresponding to a BER $<10^{-9}$ and an asymmetric shape due to the relaxation of the cavity. On the other hand, the self-mode case shows a closed eye diagram and presents a more symmetric shape, closer to the pump shape. We attribute the deterioration of the signal quality to the optical interference between the probe and pump : even though the pump and probe pulses are temporally overlapping after the device and on the detector, the optical phase of the two signals generated by two independent lasers is randomly drifting, leading to a random destructive or constructive interference of the pulses as seen in Fig. 6(d). In the cross-mode case, the broadened pump does not reach the filtering region of the probe and is completely removed, leading to a crosstalk-free signal, which explains the gain in receiver sensitivity at low BER.

5. Conclusion

We have successfully demonstrated that all-optical switching is possible with a multi-mode PhCN combined with an asymmetric Fano lineshape in InP. Due to the larger mode volume and increased cavity relaxation time, we operated the switch at 2.5 Gbps, lower than previous demonstrations for single-mode H0 cavity [25] and photonic molecules [16]. However, we show a clear enhancement of the signal quality after conversion in the cross-mode configuration where the in-band crosstalk from the pump is completely suppressed due to the large spectral separation between the pump and the probe. At the same time, the energy consumption of the switch is also lowered from 534 fJ/bit to 445 fJ/bit, though this reduction might be improved if the Q/V ratio of the pump modes in both configurations was the same. Theses improvements are not inherent to the cavity design but to the cross-mode scheme and could be applied to different cavities, with for example a smaller mode volume or an embedded PIN junction to sweep-out the carriers, so that to enhance the speed of the switch.

Funding. European Research Council (834410-FANO); Villum Fonden (8692).

Optics EXPRESS

Disclosures. The authors declare no conflicts of interest.

Data availability. Data underlying the results presented in this paper are not publicly available at this time but may be obtained from the authors upon reasonable request.

Supplemental document. See Supplement 1 for supporting content.

References

1. A. Rodriguez, J. D. Joannopoulos, J. Bravo-Abad, M. Soljačić, P. Bermel, and S. G. Johnson, "Enhanced nonlinear optics in photonic-crystal microcavities," Opt. Express **15**(24), 16161–16176 (2007).
2. K. Nozaki, T. Tanabe, A. Shinya, S. Matsuo, T. Sato, H. Taniyama, and M. Notomi, "Sub-femtojoule all-optical switching using a photonic-crystal nanocavity," Nat. Photonics **4**(7), 477–483 (2010).
3. A. E. Willner, S. Khaleghi, M. R. Chitgarha, and O. F. Yilmaz, "All-optical signal processing," J. Lightwave Technol. **32**(4), 660–680 (2014).
4. T. Tanabe, M. Notomi, S. Mitsugi, A. Shinya, and E. Kuramochi, "All-optical switches on a silicon chip realized using photonic crystal nanocavities," Appl. Phys. Lett. **87**(15), 151112 (2005).
5. A. Shinya, E. Kuramochi, G. Kira, M. Notomi, S. Mitsugi, and T. Tanabe, "Optical bistable switching action of Si high-Q photonic-crystal nanocavities," Opt. Express **13**(7), 2678–2687 (2005).
6. D. A. Bekele, Y. Yu, H. Hu, P. Guan, L. Ottaviano, M. Galili, L. K. Oxenløwe, K. Yvind, and J. Mork, "Pulse carving using nanocavity-enhanced nonlinear effects in photonic crystal fano structures," Opt. Lett. **43**(4), 955–958 (2018).
7. T. N. Nguyen, M. Gay, K. Lengle, L. Bramerie, M. Thual, J. C. Simon, S. Malaguti, G. Bellanca, S. Trillo, S. Combrie, G. Lehoucq, and A. De Rossi, "100-Gb/s wavelength division demultiplexing using a photonic crystal four-channel drop filter," IEEE Photonics Technol. Lett. **25**(9), 813–816 (2013).
8. D. A. Bekele, Y. Yu, H. Hu, P.-Y. Bony, L. Ottaviano, L. K. Oxenlowe, K. Yvind, and J. Mork, "Optical time domain demultiplexing using Fano resonance in InP photonic crystals," in *2017 CLEO/Europe-EQEC)*, (IEEE, 2017), p. 1.
9. Y. Yu, M. Heuck, H. Hu, W. Xue, C. Peucheret, Y. Chen, L. K. Oxenløwe, K. Yvind, and J. Mørk, "Fano resonance control in a photonic crystal structure and its application to ultrafast switching," Appl. Phys. Lett. **105**(6), 061117 (2014).
10. K. Nozaki, A. Shinya, S. Matsuo, T. Sato, E. Kuramochi, and M. Notomi, "Ultralow-energy and high-contrast all-optical switch involving fano resonance based on coupled photonic crystal nanocavities," Opt. Express **21**(10), 11877–11888 (2013).
11. C. Ott, A. Kaldun, P. Raith, K. Meyer, M. Laux, J. Evers, C. H. Keitel, C. H. Greene, and T. Pfeifer, "Lorentz meets Fano in spectral line shapes: A universal phase and its laser control," Science **340**(6133), 716–720 (2013).
12. M. F. Limonov, M. V. Rybin, A. N. Poddubny, and Y. S. Kivshar, "Fano resonances in photonics," Nat. Photonics **11**(9), 543–554 (2017).
13. S. Fan, "Sharp asymmetric line shapes in side-coupled waveguide-cavity systems," Appl. Phys. Lett. **80**(6), 908–910 (2002).
14. Y. Yu, H. Hu, L. K. Oxenløwe, K. Yvind, and J. Mork, "Ultrafast all-optical modulation using a photonic-crystal fano structure with broken symmetry," Opt. Lett. **40**(10), 2357–2360 (2015).
15. K. Nozaki, E. Kuramochi, A. Shinya, and M. Notomi, "25-channel all-optical gate switches realized by integrating silicon photonic crystal nanocavities," Opt. Express **22**(12), 14263 (2014).
16. S. Combrié, G. Lehoucq, A. Junay, S. Malaguti, G. Bellanca, S. Trillo, L. Ménager, J. P. Reithmaier, and A. D. Rossi, "All-optical signal processing at 10 GHz using a photonic crystal molecule," Appl. Phys. Lett. **103**(19), 193510 (2013).
17. B. R. Bennett, R. A. Soref, and J. A. Del Alamo, "Carrier-Induced Change in Refractive Index of InP, GaAs, and InGaAsP," IEEE J. Quantum Electron. **26**(1), 113–122 (1990).
18. Y. Yu, W. Xue, H. Hu, L. K. Oxenløwe, K. Yvind, and J. Mork, "All-optical switching improvement using photonic-crystal fano structures," IEEE Photonics J. **8**(2), 1–8 (2016).
19. L. Constans, S. Combrié, D. Sanchez, F. Raineri, and A. de Rossi, "All-optical sampling of a 40 ghz signal using hybrid silicon nanophotonics," Advanced Photonics 2018 (BGPP, IPR, NP, NOMA, Sensors, Networks, SPPCom, SOF) p. IM3B.4 (2018).
20. D. A. Bekele, Y. Yu, H. Hu, Y. Ding, A. Sakanas, L. Ottaviano, E. Semenova, L. K. Oxenløwe, K. Yvind, and J. Mork, "Photonic crystal Fano resonances for realizing optical switches, lasers, and non-reciprocal elements," in *Active Photonic Platforms IX*, vol. 10345 International Society for Optics and Photonics (SPIE, 2017), pp. 107–113.
21. A. D. Osterkryger, J. R. de Lasson, M. Heuck, Y. Yu, J. Mørk, and N. Gregersen, "Spectral symmetry of fano resonances in a waveguide coupled to a microcavity," Opt. Lett. **41**(9), 2065–2068 (2016).
22. S.-H. Kim and Y.-H. Lee, "Symmetry relations of two-dimensional photonic crystal cavity modes," IEEE J. Quantum Electron. **39**(9), 1081–1085 (2003).
23. W. Suh, Z. Wang, and S. Fan, "Temporal coupled-mode theory and the presence of non-orthogonal modes in lossless multimode cavities," IEEE J. Quantum Electron. **40**(10), 1511–1518 (2004).
24. C. Husko, A. De Rossi, S. Combrí, Q. V. Tran, F. Raineri, and C. W. Wong, "Ultrafast all-optical modulation in GaAs photonic crystal cavities," Appl. Phys. Lett. **94**(2), 021111 (2009).

Optics EXPRESS

25. Y. Yu, E. Palushani, M. Heuck, N. Kuznetsova, P. T. Kristensen, S. Ek, D. Vukovic, C. Peucheret, L. K. Oxenløwe, S. Combrié, A. de Rossi, K. Yvind, and J. Mørk, "Switching characteristics of an InP photonic crystal nanocavity: Experiment and theory," Opt. Express **21**(25), 31047 (2013).
26. P. Lunnemann, Y. Yu, K. Joanesarson, and J. Mørk, "Ultrafast parametric process in a photonic-crystal nanocavity switch," Phys. Rev. A **99**(5), 053835 (2019).
27. Q. Saudan, D. A. Bekele, A. Marchevsky, Y. Yu, L. K. Oxenløwe, K. Yvind, J. Mørk, and M. Galili, "Low-power thermo-optic switching using photonic crystal fano structure with p-i-n junction," in *2019 21st International Conference on Transparent Optical Networks (ICTON)*, (2019), pp. 1–4.
28. G. Moille, S. Combrié, L. Morgenroth, G. Lehoucq, F. Neuilly, B. Hu, D. Decoster, and A. de Rossi, "Integrated all-optical switch with 10 ps time resolution enabled by ALD," Laser Photonics Rev. **10**(3), 409–419 (2016).